



Convergent close-coupling approach to ion collisions with multi-electron targets: Application to $\bar{p} + \text{C}$ collisions

N. W. Antonio ^{1,*} and A. S. Kadyrov ^{1,2}

¹*Department of Physics and Astronomy, Curtin University, GPO Box U1987, Perth, WA 6845, Australia*

²*Institute of Nuclear Physics, Ulugbek, 100214 Tashkent, Uzbekistan*

(Dated: July 22, 2025)

The single-centre convergent close-coupling approach to ion-atom collisions has been extended to model collisions involving arbitrary multi-electron atoms and partially stripped ions. This is accomplished by generating a set of target pseudostates using the configuration interaction method. The resulting pseudostates are expanded in terms of configuration state functions, constructed using a hybrid of Hartree-Fock and Coulomb-Sturmian spin-orbitals. This new approach is applied to study antiproton collisions with atomic carbon. We present excitation energies, oscillator strengths, and the dipole polarisability obtained using the target structure model to validate its accuracy. Furthermore, we present results for elastic-scattering, total excitation, and ionisation cross sections in the incident energy range between 10 to 1000 keV. State-resolved excitation cross sections for the first few dominant transitions are also presented. Throughout the manuscript, we compare results obtained using the multi-core target structure model with those from a frozen-core one. In all cases, we find that a multi-core description of the carbon atom target is essential for accurately modelling these collisions.

I. INTRODUCTION

Collisions between heavy ions and multi-electron atoms or ions occur in many practical settings. They take place within fusion reactors during their operation [1], in astrophysical plasmas [2] and during hadron therapy for cancer treatment [3]. An accurate and comprehensive set of cross section data for these fundamental processes is essential for the continued development and optimization of such technologies. Hadron therapy uses high-energy heavy ions to deliver a concentrated dose of radiation to the tumour while minimizing damage to the surrounding healthy tissue [4]. This contrasts with traditional X-ray therapy, which irradiates the tumour but deposits most of the dose into healthy tissue upon entry into the body. The key advantage of hadron therapy lies in the fact that heavy ions deposit most of their energy in the region of the Bragg peak towards the end of their range. The depth at which the Bragg peak occurs can be tuned, allowing clinicians to target tumours located at different depths within the body. To accurately configure where the Bragg peak occurs, and therefore the region where the maximum radiation dose is deposited, extensive treatment planning including depth-dose simulations is required [4]. The accuracy of these simulations is paramount in ensuring the effectiveness of the treatment. However, the primary limiting factor in their accuracy is the lack of accurate cross section data for the underlying ion collisions. Therefore, both calculating and measuring these cross sections is of utmost importance to the continued advancement of hadron therapy.

There are many different types of ions that can be used as beams for hadron therapy, and there is active research

into various candidate ions for future applications [5]. In fact, proton and carbon ion therapy are currently in use for treatment today. One particularly interesting candidate ion that has been proposed for use in hadron therapy is the antiproton [6]. Antiprotons exhibit an additional effect, compared to positive ions, due to their annihilation at the end of their range. This annihilation process results in approximately 2.75 times more energy being deposited at the tumour site compared to proton and carbon ions [6]. Despite these promising benefits of antiproton therapy, it remains in the experimental phase. However, research into the use of antiprotons in hadron therapy is ongoing [7, 8].

In reality, ions used in hadron therapy collide with complex molecules within the human body, such as DNA and proteins, which are composed of many atoms. Modelling collisions with such targets in a completely *ab initio* manner is currently infeasible due to the complexity of the problem. However, current approaches to effectively model such collisions involve using the so-called independent atom model (IAM) [9]. Applying the IAM to compute cross sections relies on accurate calculations of ion collisions with the corresponding atoms that constitute the molecular targets. One of the most important biologically relevant atomic targets is carbon, as it is a primary constituent of organic molecules, and is therefore present in all biological systems.

Significant progress has been made in the past few decades on modelling ion collisions with one- and two-electron targets, in particular. A number of different theoretical approaches currently exist to model such collisions. These include the classical trajectory Monte Carlo (CTMC) [10], continuum distorted wave (CDW) [11], molecular orbital close-coupling (MOCC) [12], atomic orbital close-coupling (AOCC) [13], and lattice numerical solution of the time-dependent Schrödinger

* nicholas.antonio@postgrad.curtin.edu.au

equation (LTDSE) [14] methods. For recent reviews on the subject of ion-atom collisions, see Refs. [15–17]. The combination of these methods along with experimental measurements has provided a wealth of data for ion collisions with one- and two-electron targets. However, the situation is quite different for multi-electron targets, where accurate data is still quite limited. The primary challenge lies in accounting for the electron-electron correlation effects, and the growing number of interactions that need to be accounted for as the number of electrons in the target increases.

With recent advancements in computing resources [18], it is now becoming feasible to model ion collisions with multi-electron targets with sufficient accuracy. A notable method developed to study heavy ion collisions with multi-electron targets is the basis generator method (BGM) [19]. This approach was applied to study the energy loss in antiproton collisions with helium, carbon, nitrogen, oxygen and neon atoms in Ref. [19]. They performed two sets of calculations, one where the model potential which accounts for the electron-electron interactions is independent of the position of the projectile ion (referred to as the no-response model), and another where this potential is dependent on the position of the projectile ion (referred to as the response model) [20]. The results displayed good agreement with experimental data for the He and Ne atoms. However at the same time, no experimental or theoretical data existed for the C, N, and O atoms to compare with. Another recently developed method to study antiproton collisions with Ne and Ar atoms is a time-dependent close-coupling approach by Jia *et al.* [21]. This approach used a pseudostate basis of configuration-interaction (CI) wavefunctions built from gaussian-type orbitals.

Various quantum-mechanical (QM) and semi-classical (SC) implementations of the convergent close-coupling (CCC) approach to ion-atom collisions, using an orthogonal Laguerre, wave-packet (WP), and Coulomb-Sturmian (CS) bases have been applied to a wide range of collisions involving one- and multi-electron targets including H [22–26], He [27, 28], the inert gases [29], the alkalis [30, 31], and H₂ [32–34]. In general, the CCC framework, both in QM and SC formulations, has been able to reproduce experimental measurements with high accuracy. In this work we extend the single-centre Coulomb-Sturmian convergent close-coupling (CS-CCC) approach to ion-atom collisions to model collisions with arbitrary multi-electron targets without the need to use an effective one-electron approach. To this end we develop a new general atomic structure code based on the CI method that is capable of representing the entire spectra of any atom using the *LS* coupling scheme. Having this code developed in-house allows us to seamlessly integrate it with our existing CS-CCC scattering code to maximise the computational performance of our calculations. We use a hybrid set of spin-orbitals consisting of Hartree-Fock (HF) [35] and Coulomb-Sturmian [36] ones. These multi-electron CI

states are then used to expand the total scattering wavefunction, which upon substituting into the full Schrödinger equation, gives us a set of coupled-channel equations for the transition probability amplitudes. To demonstrate the capabilities of this new approach, we apply it to study $\bar{p} + \text{C}$ collisions. This is motivated not only for its relevance to hadron therapy, but also because it is one of the first atoms in the periodic table that requires core-excited electron configurations to build an accurate target structure model. This makes it a perfect test case for the new approach and corresponding code. We will present calculations of the total elastic-scattering, excitation, and ionisation cross sections for these collisions in the incident energy range from 10 to 1000 keV. Furthermore, we will present results for some of the dominant state-resolved excitation cross sections for transitions from the *2s* and *2p* shells.

The remainder of this manuscript is structured as follows. In Sec. II we present our theoretical approach to model $\bar{p} + \text{C}$ collisions. In Sec. III we present details of our calculations, including details of the target structure model and numerical parameters required to obtain converged results. In Sec. IV we present the results of our calculations, and finally in Sec. V we present our conclusions and outlook for future work.

Atomic units are used throughout this work unless otherwise stated.

II. THEORY

Details of the single-centre semi-classical CCC approach to ion-atom collisions have been discussed in previous works, see e.g. [37, 38]. Therefore, a brief overview of the scattering part of the theory will be presented here. The focus of this section will be on incorporation of the multi-electron atomic structure model into the CS-CCC approach. Furthermore, as we are interested in collisions in the incident energy range between 10 to 1000 keV, we describe $\bar{p} + \text{C}$ collisions using the single-centre approach.

A. Target structure

For generality, let us consider some arbitrary *N*-electron target atom or ion with a corresponding Hamiltonian H_T , given by

$$H_T = \sum_{i=1}^N \left(-\frac{1}{2} \nabla_i^2 - \frac{Z_T}{r_i} \right) + \sum_{i < j}^N \frac{1}{|\mathbf{r}_i - \mathbf{r}_j|}, \quad (1)$$

where Z_T is the charge of the target nucleus, and \mathbf{r}_i (\mathbf{r}_j) is the position of the *i*-th (*j*-th) electron relative to the nucleus. We construct each *N*-electron pseudostate $|\psi_\alpha\rangle$ of the target using the CI method. Furthermore, we use the *LS*-coupling scheme to label the atomic states. This way, the good quantum numbers needed to describe

the states are the total orbital angular momentum L , its projection M , the total spin S , its projection Σ and the parity Π . Including an index n to distinguish between states with the same set of quantum numbers, we use the label α to represent the following set $\{n, L, M, S, \Sigma, \Pi\}$ for the pseudostate $|\psi_\alpha\rangle$. Each pseudostate is expanded in terms of a set of configuration state functions (CSFs) represented by $|j : L, M, S, \Sigma, \Pi\rangle$ as follows

$$|\psi_\alpha\rangle = \sum_{j=1}^{M_{LS\Pi}} c_j^{(\alpha)} |j : L, M, S, \Sigma, \Pi\rangle, \quad (2)$$

where $M_{LS\Pi}$ is the number of CSFs used to expand the pseudostate $|\psi_\alpha\rangle$, which differs depending on the quantum numbers L , S and Π . For the remainder of this work, for brevity, we may often omit the magnetic quantum numbers M and Σ from the notation of the CSFs, and assume that they are implicitly present. The CI coefficients, denoted as $c_j^{(\alpha)}$, are determined by diagonalising the target Hamiltonian H_T in the space spanned by the chosen set of CSFs. Index j represents a single electron configuration $\{(n_1, l_1), (n_2, l_2), \dots, (n_N, l_N)\}$, as well as a unique set of intermediate orbital and spin angular momentum couplings. The CSFs are constructed in such a way that they are eigenstates of \hat{L}^2 and \hat{S}^2 , where \hat{L} and \hat{S} are the operators of the total orbital angular momentum and total spin, respectively, along with the projection operators \hat{L}_z and \hat{S}_z . This is achieved by writing each CSF as a linear combination of Slater determinants $|\chi_{j_1}, \dots, \chi_{j_N}\rangle$ with appropriate coefficients as follows

$$|j : L, S, \Pi\rangle = \sum_{\mu_j \in \Gamma_j} A_{\mu_j}^{(L, S, \Pi)} |\chi_{j_1}, \dots, \chi_{j_N}\rangle, \quad (3)$$

where μ_j is a set of one-electron projection quantum numbers $\{(m_1, \sigma_1), (m_2, \sigma_2), \dots, (m_N, \sigma_N)\}$ and Γ_j is the collection of all possible sets of one-electron projection quantum numbers for the j -th electron configuration. For clarity, we collect all four one-electron quantum numbers for the i -th electron into a single index j_i . To help articulate the index notation we use, refer to a schematic diagram in Fig. 1 which illustrates the mappings between the various indices used to define electron configurations. The coefficients $A_{\mu_j}^{(L, S, \Pi)}$ are the angular momentum coupling ones which are determined by coupling each of the N -electron orbital angular momenta ℓ_{j_i} and spins σ_{j_i} , along with their associated projection quantum numbers.

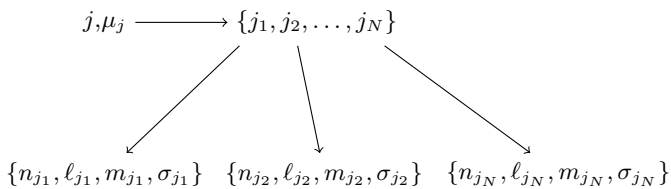


FIG. 1. Schematic diagram of the indexing used to label the N -electron configurations.

The Slater determinants can be written as antisymmetrised products of one-electron spin-orbitals $|\chi_{j_i}\rangle$ as follows

$$|\chi_{j_1}, \chi_{j_2}, \dots, \chi_{j_N}\rangle = \frac{1}{\sqrt{N!}} \mathcal{A} |\chi_{j_1}\rangle |\chi_{j_2}\rangle \dots |\chi_{j_N}\rangle, \quad (4)$$

where \mathcal{A} is the antisymmetrisation operator.

Defining \mathbf{x} as the position and spin of the i -th electron, we can write the spin-orbital in the position representation as follows

$$\chi_{j_i}(\mathbf{x}) = \frac{1}{r} \varphi_{n_i \ell_i}(r) Y_{\ell_i m_i}(\hat{\mathbf{r}}) X_{\frac{1}{2}}(\sigma_i), \quad (5)$$

where in general $\varphi_{n_i \ell_i}(r)$ is some square-integrable radial function, $Y_{\ell_i m_i}(\hat{\mathbf{r}})$ is spherical harmonics, and $X_{\frac{1}{2}}(\sigma_i)$ is a spin function. It is worth mentioning that the choice of the radial functions $\varphi_{n_i \ell_i}(r)$ is very important as it strongly influences the convergence rate of the CI calculations with increasing the size of the expansion ($M_{LS\Pi}$). To best describe the low-lying states of the target atom, while also maintaining adequate representation of the continuum, we use a hybrid set of radial functions consisting of HF and CS ones. The HF radial functions are generated using the program by Froese Fischer [39]. The present structure code is written in such a way that the spin-orbitals do not need to be orthogonal to each other, allowing for further flexibility in the choice of the radial functions.

The CI coefficients $c_j^{(\alpha)}$ and associated energy eigenvalues ε_α can be obtained by solving the following generalized eigenvalue problem for each L , S and Π needed for convergence of the subsequent scattering calculations:

$$\sum_{j=1}^{M_{LS\Pi}} \left(H_{ij}^{(L, S, \Pi)} - \varepsilon_\alpha S_{ij}^{(L, S, \Pi)} \right) c_i^{(\alpha)} = 0, \quad (6)$$

where $H_{ij}^{(L, S, \Pi)}$ and $S_{ij}^{(L, S, \Pi)}$ are the Hamiltonian and overlap matrix elements between the CSFs which can be written in terms of matrix elements between the Slater determinants as follows

$$\begin{aligned} S_{ij}^{(L, S, \Pi)} &= \sum_{\mu_i \mu_j} A_{\mu_i}^{(L, S, \Pi)} A_{\mu_j}^{(L, S, \Pi)} \langle \chi_{i_1}, \dots, \chi_{i_N} | \chi_{j_1}, \dots, \chi_{j_N} \rangle, \\ H_{ij}^{(L, S, \Pi)} &= \sum_{\mu_i \mu_j} A_{\mu_i}^{(L, S, \Pi)} A_{\mu_j}^{(L, S, \Pi)} \langle \chi_{i_1}, \dots, \chi_{i_N} | H_T | \chi_{j_1}, \dots, \chi_{j_N} \rangle. \end{aligned} \quad (7)$$

We evaluate the matrix elements between various Slater determinants using the generalized Slater-Condon rules [40].

B. Semi-classical convergent close-coupling approach

Let us consider a collision between an ion with charge Z_P , and an N -electron target atom. The Hamiltonian

for the collision system can be written as

$$H = K_{\sigma} + H_T + \bar{V}, \quad (8)$$

where K_{σ} is the kinetic energy operator for the relative motion of the incoming antiproton projectile and the target atom, making σ the position of the antiproton relative to the target atom. The operator \bar{V} represents the interaction potential between the antiproton and the target atom which can be written as

$$\bar{V} = \frac{Z_P Z_T}{R} - Z_P \sum_{i=1}^N \frac{1}{|\mathbf{r}_i - \mathbf{R}|}, \quad (9)$$

where \mathbf{R} is the position of the antiproton relative to the target nucleus. As the Hamiltonian of the collision system is independent of the electron spin, it is trivial to show that the total spin of the system is conserved. Therefore, for the remainder of this section for brevity, we drop the initial spin of the target S and its projection being Σ from the notation. We wish to find solutions to the full Schrödinger equation of the collision system

$$(H - E)\Psi_i^+(\sigma, \mathbf{x}_1, \dots, \mathbf{x}_N) = 0, \quad (10)$$

where E is the total energy of the collision system, superscript $+$ indicates the scattering wavefunction has outgoing-wave boundary conditions, and i specifies the initial state of the target atom. In order to solve Eq. (10), we expand the total scattering wavefunction Ψ_i^+ in terms of N_T target pseudostates ψ_{α} as follows

$$\Psi_i^+(\sigma, \mathbf{x}_1, \dots, \mathbf{x}_N) \approx \sum_{\alpha=1}^{N_T} \mathcal{F}_{\alpha}(\sigma) e^{i\mathbf{k}_{\alpha} \cdot \sigma} \psi_{\alpha}(\mathbf{x}_1, \dots, \mathbf{x}_N), \quad (11)$$

where \mathbf{k}_{α} is the relative momentum between the antiproton and the target atom, and $\mathcal{F}_{\alpha}(\sigma)$ are initially unknown expansion coefficients.

Inserting the expansion for the Ψ_i^+ into Eq. (10) and projecting it by N_T asymptotic states, $e^{i\mathbf{k}_{\alpha'} \cdot \sigma} \psi_{\alpha'}$, we are able to obtain a set of coupled-channel equations for the unknown coefficients. To make the set numerically tractable, we employ the semi-classical approximation. This approximation, models the motion of the incoming antiproton using a classical trajectory, while leaving the electron dynamics described fully quantum-mechanically. This allows us to write $\mathbf{R} \equiv \mathbf{R}(t, \mathbf{b}) = \mathbf{b} + \mathbf{v}t$, where \mathbf{b} is the impact parameter, \mathbf{v} is the initial velocity of the antiproton, and t is the time. The time parameterisation is defined such that $t = -\infty$ corresponds to the moment prior to the collision, $t = 0$ corresponds to the moment of the closest approach, and $t = +\infty$ corresponds

to time after the collision. Next we Taylor expand the coefficients \mathcal{F}_{α} about \mathbf{R} . Safely assuming that second and higher order terms in the expansion are negligible, we can write the coefficients as functions of \mathbf{R} , like $\mathcal{F}_{\alpha}(\sigma) \approx F_{\alpha}(t, \mathbf{b})$. Next, the semi-classical approximation is applied, reducing the coupled-channel equations to

$$i \frac{dF_{\alpha'}(t, \mathbf{b})}{dt} = \sum_{\alpha=1}^{N_T} F_{\alpha}(t, \mathbf{b}) \langle \psi_{\alpha'} | \bar{V} | \psi_{\alpha} \rangle e^{iv(k_{\alpha} - k_{\alpha'})t}, \quad (12)$$

where the index α' runs from 1 to N_T . These close-coupling (CC) equations are solved with the initial condition

$$F_{\alpha}(t = -\infty, \mathbf{b}) = \delta_{\alpha i}, \quad (13)$$

for all α from 1 to N_T . In this work, i is set to correspond to the ground $1s^2 2s^2 2p^2 {}^3P^e$ state of the carbon atom with different initial total magnetic quantum numbers $M = 0, \pm 1$.

In order to solve the set of Eqs. (12), we need to first evaluate the scattering matrix elements $\langle \psi_{\alpha'} | \bar{V} | \psi_{\alpha} \rangle$. To do this, we first expand them in terms of matrix elements between the CSFs $\langle i : L', M', \Pi' | \bar{V} | j : L, M, \Pi \rangle$ ¹, as follows

$$\langle \psi_{\alpha'} | \bar{V} | \psi_{\alpha} \rangle = \sum_{ij} c_i^{(\alpha')} c_j^{(\alpha)} \langle i : L', M', \Pi' | \bar{V} | j : L, M, \Pi \rangle. \quad (14)$$

Next, we partial-wave expand the interaction potential as follows

$$\bar{V}(\mathbf{R}, \mathbf{r}_1, \dots, \mathbf{r}_N) = \sum_{\lambda\mu} \bar{V}_{\mu}^{(\lambda)}(R, \mathbf{r}_1, \dots, \mathbf{r}_N) C_{\mu}^{(\lambda)*}(\hat{\mathbf{R}}), \quad (15)$$

where $C_{\mu}^{(\lambda)}(\hat{\mathbf{R}})$ are the renormalised spherical harmonics as defined in Ref. [35] and $\bar{V}_{\mu}^{(\lambda)}(R, \mathbf{r}_1, \dots, \mathbf{r}_N)$ is given by

$$\bar{V}_{\mu}^{(\lambda)}(R, \mathbf{r}_1, \dots, \mathbf{r}_N) = Z_P \sum_{k=1}^N \mathcal{U}_{\lambda}(r_k, R) Y_{\lambda\mu}(\hat{\mathbf{r}}_k). \quad (16)$$

The functions $\mathcal{U}_{\lambda}(r_k, R)$ are written as

$$\mathcal{U}_{\lambda}(r_k, R) = \begin{cases} \frac{Z_T}{R} \delta_{\lambda 0} - \frac{r_k^{\lambda}}{R^{\lambda+1}}, & \text{if } r_k \leq R, \\ \frac{Z_T}{R} \delta_{\lambda 0} - \frac{R^{\lambda}}{r_k^{\lambda+1}}, & \text{if } r_k > R. \end{cases} \quad (17)$$

Substituting the expansion given in Eq. (15) and applying the Wigner-Eckart theorem, the matrix elements in Eq. (12) reduce to

dependent on these numbers.

¹ Here, we explicitly show the magnetic quantum numbers M' and M of the CSFs to emphasise that these matrix elements are

$$\langle \psi_{\alpha'} | \bar{V} | \psi_{\alpha} \rangle = \sum_{ij\lambda} c_i^{(\alpha')} c_j^{(\alpha)} C_{L,M,\lambda,\mu}^{L',M'} \langle i : L', \Pi' | \bar{V}_{\mu}^{(\lambda)} | j : L, \Pi \rangle C_{\mu}^{(\lambda)*}(\hat{R}), \quad (18)$$

where $C_{L,M,\lambda,\mu}^{L',M'}$ is a Clebsch-Gordan coefficient, and $\langle i : L', \Pi' | \bar{V}_{\mu}^{(\lambda)} | j : L, \Pi \rangle$ is a reduced matrix element, independent of the magnetic quantum numbers, for the transition between the two CSFs.

To evaluate the reduced matrix elements in Eq. (18), we first evaluate the corresponding matrix elements that depend on the magnetic quantum numbers, $\langle i : L', M', \Pi' | \bar{V}_{\mu}^{(\lambda)} | j : L, M, \Pi \rangle$, for any given values of M' and M . The best choice of the magnetic quantum numbers to use to evaluate these matrix elements is $M' = L'$ and $M = L$, as these are the ones which minimise the number of Slater determinants needed to construct each corresponding CSF. The evaluation of the

full matrix elements is done similarly to what is done for the Hamiltonian and overlap matrix elements in Eq. (7). Specifically, we first expand the CSFs in terms of their respective Slater determinants to get

$$\begin{aligned} \langle i : L', M', \Pi' | \bar{V}_{\mu}^{(\lambda)} | j : L, M, \Pi \rangle = \\ \sum_{\mu_i \mu_j} A_{\mu_i}^{(L', S, \Pi')} A_{\mu_j}^{(L, S, \Pi)} \langle \chi_{j_1}, \dots, \chi_{j_N} | \bar{V}_{\mu}^{(\lambda)} | \chi_{j_1}, \dots, \chi_{j_N} \rangle. \end{aligned} \quad (19)$$

After applying the generalised Slater-Condon rules to determine the matrix elements between the Slater determinants and using Eq. (16), we get the final expression for the full matrix elements in terms of the one-electron matrix elements as follows

$$\langle i : L', M', \Pi' | \bar{V}_{\mu}^{(\lambda)} | j : L, M, \Pi \rangle = Z_P \sum_{\mu_i \mu_j ab} (-1)^{(a+b)} A_{\mu_i}^{(L', S, \Pi')} A_{\mu_j}^{(L, S, \Pi)} \langle \chi_{i_a} | \mathcal{U}_{\lambda}(r, R) | \chi_{j_b} \rangle |S(i, j|a, b)|, \quad (20)$$

where $\langle \chi_{i_a} | \mathcal{U}_{\lambda}(r, R) | \chi_{j_b} \rangle$ is the one-electron matrix element between the spin-orbitals χ_{i_a} and χ_{j_b} which can be evaluated as shown in previous works such as in Ref. [22]. The term $S(i, j|a, b)$ is the matrix of one-electron overlaps between all the spin orbitals from electron configuration i and j with row a and column b removed, making $|S(i, j|a, b)|$ its determinant. With these matrix elements known, we can then apply an inverse application of the Wigner-Eckart theorem to obtain the reduced matrix elements $\langle i : L', \Pi' | \bar{V}_{\mu}^{(\lambda)} | j : L, \Pi \rangle$. As evaluating Eq. (20) is computationally expensive, following the procedure outlined above we are able to drastically speed up the calculations by only needing to calculate magnetic quantum number-dependent matrix elements for only one pair of M' and M for each CSF pair.

C. Cross sections

It has been shown in Ref. [30], that in the limit of $t \rightarrow +\infty$, the expansion coefficients $F_{\alpha}(+\infty, \mathbf{b})$ represent the transition probability amplitudes in the impact parameter representation. As a result, the probability of transition from some initial state i to some final state

f can be calculated as follows

$$P_{fi}^{(M_f, M_i)}(b) = |F_f(+\infty, \mathbf{b}) - \delta_{fi}|^2, \quad (21)$$

where the superscript (M_f, M_i) indicates that the transition probabilities are fully state-resolved, i.e. they depend on the magnetic quantum numbers M_f and M_i of the final and initial states, respectively. The corresponding total cross section for the transition can be calculated by integrating the transition probabilities with respect to the parameter \mathbf{b} as follows

$$\sigma_{fi}^{(M_f, M_i)} = 2\pi \int_0^{+\infty} b P_{fi}^{(M_f, M_i)}(b) db. \quad (22)$$

If the initial state of the target atom has $L_i > 0$, then there are $2L_i + 1$ degenerate states with the same energy. As a result, we can define excitation cross sections independent of the magnetic quantum numbers by averaging over all the initial-state magnetic quantum numbers and summing over the final ones as follows

$$\sigma_{fi} = \frac{1}{2L_i + 1} \sum_{M_i M_f} \sigma_{fi}^{(M_f, M_i)}. \quad (23)$$

All results presented in this work are averaged over the initial state magnetic quantum numbers according to Eq. (23).

III. DETAILS OF THE CALCULATIONS

A. Target structure model

Before scattering calculations can be performed, we need to first construct a atomic structure model which can adequately represent the spectrum of the carbon atom target. To begin with, we performed HF calculations for the ground state of the carbon atom. This produced a set of radial orbitals corresponding to the $1s$, $2s$ and $2p$ subshells. The remaining spin orbitals were constructed using the CS radial functions, with falloff parameter set to 1.0. To account for the correlations between the valence electrons, we included configurations of the form $1s^2 2s^2 n\ell n'\ell'$. Depending on the term symbol $2S+1L^\Pi$ the range of n , ℓ , and ℓ' were different. In summary, across all symmetries considered, n went up to at most 9 and ℓ went up to at most 3 depending on the term symbol of the configuration, while n' went up to 18 in all cases and ℓ' went up to at most 4. From here on, we define the maximum value of n' used in the model as n_{\max} . In addition, to account for the correlations between the valence and core electrons, we included the following set of electron configurations: $1s^2 2p^2 n\ell n'\ell'$, $1s^2 2s 2p n\ell n'\ell'$ and $1s^2 2s (n\ell)^3$. Just as for the valence-valence electron configurations, in all cases n' went up to n_{\max} and the range of n , ℓ and ℓ' depended on the term symbol and specific type of electron configuration with the same range as specified above.

Throughout the manuscript we compare results obtained using a frozen-core (FC) and multi-core (MC) description of the carbon atom. This is to emphasise the necessity to describe the C structure using the MC description, as well as the importance of the core-valence electron correlations. The FC approach only includes electron configurations of the following form: $1s^2 2s^2 2p n\ell$, where the maximum value of n was n_{\max} and ℓ went up to at most 4. The excitation energies of the first few states of C obtained using both the FC and MC approaches is presented in Table I. Alongside these energies we also show the ones given in the NIST database [41]. The last column shows the percentage difference between the present MC results and the NIST data. Firstly, we note that the largest difference between the present FC and MC calculations, which is 8%, appears to be for the $2s^2 2p 3p \ ^3P^e$ state. Another interesting observation is that while the energies of the $2s^2 2p 3p \ ^3P^e$, $2s^2 2p 3p \ ^3S^e$ and $2s^2 2p 3p \ ^3D^e$ states in the MC model are almost degenerate, they still appear to require the multi-core CSFs to be accurately described. This is seen by comparing their respective energies in the FC and MC calculations. The largest difference between the NIST data and these first several states of the atom obtained in the MC model is 2.53% and that is for the $2s^2 2p 4s \ ^3P^o$ state. However, for modelling $\bar{p} + C$ collisions, this level of accuracy is acceptable.

When working on atomic collision problems with

methods such as coupled-channel ones, it is not feasible to reach the level of precision in the structure models similar to that required in quantum chemistry studies [42]. This is because we need to balance the accuracy of the first few bound states while still being able to adequately represent the continuum using a reasonable number of pseudostates. To this effect, in Table II we present a comparison between the present CI structure model excitation energies obtained using the MC approach and other CI calculations used in other atomic collision theory works. It is generally considered that the model of C by Wang *et al.* [43], used to study $e^- + C$ collisions, is the most accurate one to compare to in the context of modelling collisions involving the carbon atom [44]. It was generated using the B-spline R-matrix codes by Zatsarinny [45]. One of the main strengths of the Zatsarinny code is that it is capable of using term-dependent sets of spin orbitals. This means that in their approach, the radial functions can be optimised for each term symbol. The functions used in Ref. [43] was comprised of a set of multi-configurational Hartree-Fock (MCHF) radial ones for the C atom and B-spline functions. It is not explicitly stated how the set of radial functions used by Stancalie [44] was generated. Generally, we find our excitation energies align closer to the benchmark one by Wang *et al.* [43] than the Stancalie [44].

Aside from the set of excitation energies generated by the CI calculations, another crucial assessment of the quality of the structure model is the set of oscillator strengths it produces. In Table III we show the present oscillator strengths for transitions from the ground state of the C atom to the first few excited states alongside other calculated values from the same works as in Table II. Also shown are the corresponding NIST values [41] for comparison. Generally, we find that our results agree well with the available NIST data, with the exceptions of the transitions to the $2s 2p^2 4s \ ^3P^o$ and $2s^2 2p 3d \ ^3P^o$ states. Excluding the previous two transitions, we also find our results agree well with the benchmark ones by Wang *et al.* [43]. However, the results by Stancalie [44] are generally further away from the Wang *et al.* results and our present calculations, as well as the NIST data.

The last quality check we perform on the present structure model is to compare the dipole polarisability of the ground state of the C atom with the accepted value. Our model produces a value of $11.66 a_0^3$, which is within 3% of the accepted value of $11.3 \pm 0.2 a_0^3$ reported in Ref. [46]. Furthermore, this value is close to the one by Wang *et al.* [43] which is $11.31 a_0^3$. It is important to emphasise that we are not only concerned with obtaining an accurate description of the bound state spectrum of the C atom, but also of the continuum. The obtained result for the dipole polarisability is an indication that our new structure model adequately represents the continuum in addition to the bound state spectrum.

With all of the above quality checks performed, we can

State	Term	Present (FC)	Present (MC)	NIST [41]	% diff
$2s^2 2p^2$	$^3P^e$	0.0000	0.0000	0.0000	0.000
$2s^2 2p3s$	$^3P^o$	0.2951	0.2758	0.2749	0.33
$2s2p^3$	$^3D^o$	-	0.2937	0.2920	0.58
$2s^2 2p3p$	$^3D^e$	0.3342	0.3235	0.3175	1.89
$2s^2 2p3p$	$^3S^e$	0.3406	0.3236	0.3223	0.43
$2s^2 2p3p$	$^3P^e$	0.3477	0.3235	0.3251	0.49
$2s2p^3$	$^3P^o$	-	0.3429	0.3429	0.00
$2s^2 2p4s$	$^3P^o$	0.3750	0.3649	0.3559	2.53
Ionis. Limit		0.4118	0.4172	0.4138	0.82
$2s2p^3$	$^3S^o$	-	0.4765	0.4821	1.16

TABLE I. Comparison of the present CI results for the excitation energies of the triplet states of the C atom with the NIST data. Both frozen-core (FC) and multi-configuration (MC) CI calculations are shown. The last column shows the percentage difference between the present MC results and the NIST data. The ionisation limit is determined by performing a CI calculation for the ground state of the C^+ ion and taking the difference between the ground state energy of the C^+ ion and the ground state energy of the C atom.

State	Term	Present (MC)	Wang <i>et al.</i> [43]	Stancalie [44]
$2s^2 2p^2$	$^3P^e$	0.0000	0.0000	0.0000
$2s^2 2p3s$	$^3P^o$	0.2758	0.2766	0.2720
$2s2p^3$	$^3D^o$	0.2937	0.2941	0.3065
$2s^2 2p3p$	$^3D^e$	0.3235	0.3178	0.3160
$2s^2 2p3p$	$^3S^e$	0.3236	0.3225	0.3224
$2s^2 2p3p$	$^3P^e$	0.3235	0.3255	0.3421
$2s2p^3$	$^3P^o$	0.3429	0.3446	0.3497
$2s^2 2p4s$	$^3P^o$	0.3649	0.3554	0.3727
Ionis. Limit		0.4172	-	
$2s2p^3$	$^3S^o$	0.4765	0.4804	0.4821

TABLE II. Same as Table I but the present MC CI results are compared with the structure calculations from Wang *et al.* [43], and Stancalie [44].

be confident that the present structure model accurately represents the spectrum of the C atom and can be used to model antiproton collisions with this atom.

B. Convergence tests and numerical parameters

Aside from the accuracy of the atomic structure model, the accuracy of subsequent close-coupling calculations also depends on the level of convergence with respect to increasing the size of the expansion of the scattering wavefunction (11). In order to ensure that the cross sections of interest converge to within a few percent, we perform the following series of convergence tests at three key incident energies: 10, 100, and 1000 keV. Firstly, we fix $n_{\max} = 18$ and establish convergence with

respect to the number of symmetries (term symbols) included in the coupled-channel calculations, i.e. used in the expansion of the scattering wavefunction (11). To do this we begin with only including states with $^3P^e$ and $^3P^o$ symmetries. Then we continued to increase the total orbital angular momentum L , including both parities each time, until we reached $L = 4$. Therefore, the final set of close-coupling calculations included states with the following term symbols: $^3P^e$, $^3P^o$, $^3D^e$, $^3D^o$, $^3S^e$, $^3S^o$, $^3F^e$, $^3F^o$, $^3G^e$, and $^3G^o$. Having fixed the number of symmetries included in the calculations, we then established convergence with respect to increasing n_{\max} . Starting from $n_{\max} = 10$, we increased it by 2 until we reached $n_{\max} = 18$. The differences between the cross sections presented in this work using $n_{\max} = 18$ versus $n_{\max} = 16$ were less than 1% in all cases.

Transition	Wang <i>et al.</i> [43]	Stancalie [44]	Present (MC)	NIST [41]
$2s^2 2p^2 \ ^3P^e \rightarrow 2s^2 2p 3s \ ^3P^o$	0.143	0.124	0.130	0.140
$2s^2 2p^2 \ ^3P^e \rightarrow 2s 2p^3 \ ^3D^o$	0.073	0.098	0.071	0.072
$2s^2 2p^2 \ ^3P^e \rightarrow 2s 2p^3 \ ^3P^o$	0.056	0.028	0.069	0.063
$2s^2 2p^2 \ ^3P^e \rightarrow 2s 2p^2 4s \ ^3P^o$	0.027	0.023	0.016	0.021
$2s^2 2p^2 \ ^3P^e \rightarrow 2s^2 2p 3d \ ^3D^o$	0.096	0.112	0.094	0.094
$2s^2 2p^2 \ ^3P^e \rightarrow 2s^2 2p 3d \ ^3P^o$	0.037	0.340	0.016	0.040
$2s^2 2p^2 \ ^3P^e \rightarrow 2s 2p^3 \ ^3S^o$	0.156	0.171	0.143	0.152

TABLE III. The oscillator strengths for C. The present CI calculations are shown alongside the results from Wang *et al.* [43] and Stancalie [44]. The last column shows the data available from [41].

The CI calculations of the carbon atom produce a very dense set of pseudostates above the first ionisation threshold which represent its continuous spectrum. Even with today's computing resources, it is not feasible, nor necessary, to include all of them in subsequent close-coupling calculations. To reduce the number of pseudostates we do the following. We introduce a parameter denoted as ε_{\max} which specifies the maximum energy of the corresponding pseudostates to be included. We then increase this parameter until the cross sections converge to the desired accuracy. We found that incrementing ε_{\max} from 1.8 a.u. to 2.0 a.u. resulted in negligible differences in the total and state-resolved excitation cross sections and a maximum of a 4% difference in the ionisation cross section at 1000 keV. This difference decreases to less than 1% at 100 keV, and is negligible at 10 keV. In summary, our final CS-CCC calculations included 2590 pseudostates with excitation energies up to 2.0 a.u. above the ground-state energy. This is approximately two times larger than the $\varepsilon_{\max} = 1.03$ a.u. used by Wang *et al.* in Ref. [43]. Note that the value of ε_{\max} used by Wang *et al.*, is below the double ionisation threshold. Therefore, their structure model only includes positive-energy states corresponding to single ionisation. Whereas the model used in the present work includes states corresponding to both single and double ionisation.

In order to keep the number of CSFs used to expand each of the pseudostates to a reasonable number, we also used a CI coefficient cutoff parameter. In all results presented in this work, we used a cutoff of 0.0005. This means that for each pseudostate ψ_α , any CSF with electron configuration j whose corresponding CI coefficient $|c_j^{(\alpha)}| < 0.0005$ was excluded in the expansion of that particular pseudostate for the close-coupling calculations. The value of this cutoff was determined by starting from 0.01 and decreasing it incrementally until negligible differences in the results were observed. This is contrast to the CI coefficient cutoff value of 0.02 used by Wang *et al.* [43].

For a specified incident energy, the CC equations in Eq. (12) are solved for each impact parameter along a

discretised z -grid using the Runge-Kutta method, where $z = vt$ is the position of the antiproton along the z -axis at time t . The extent of this grid is defined as $[-z_{\max}, z_{\max}]$. The number of points that discretise this grid and its extent are carefully chosen to ensure that the resulting cross sections are stable with respect to varying these parameters to three significant figures. In these calculations we find that setting $z_{\max} = 100$ a.u. and discretising the z -grid into 600 exponentially distributed points (denser set of points about the $z = 0$ one) was sufficient. A vital check of the quality of our calculations is the norm of the scattering wavefunction. We ensure that, at all values of z apart of the grid, $|\Psi_i^+|^2 = 1$ to within three significant figures. The number of impact parameters used as well as the largest impact parameter, b_{\max} , varies greatly depending on the incident energy. At 10 keV, 66 impact parameter points with $b_{\max} = 15$ a.u., were required to ensure the weighted probabilities in the integrand of Eq. (22) vary smoothly and falloff a least three orders of magnitude from the maximum value. At 1000 keV, however, 94 impact parameter points with $b_{\max} = 50$ a.u. were necessary to achieve the same outcome.

IV. RESULTS AND DISCUSSION

Figure 2 presents cross sections for elastic-scattering (top panel), total excitation (middle panel) and ionisation (bottom panel) as functions of the incident projectile energy. The total excitation cross section is defined as the sum of the cross sections for excitation of all the states below the first ionisation threshold. To better understand the role the accuracy of the target structure model plays in the scattering cross sections, we present CS-CCC results obtained using both the FC and MC models. Furthermore, for comparison, we also present both FC and MC results obtained using the first Born approximation (FBA). Two previous calculations for the net ionisation cross section using the BGM method with the no-response and response approaches [19] are also shown.

We note that the CS-CCC results (both the FC and MC ones) merge with the corresponding FBA ones at the highest incident energies. However, it is clear that the CS-CCC and FBA results for the elastic-scattering cross section do not completely merge until beyond 1000 keV. We see that the CS-CCC excitation and ionisation cross sections merge with the corresponding FBA ones beyond about 300 keV.

Comparing the FC and MC cross sections resulting from the CS-CCC calculations with the corresponding FBA ones, we see minor differences in the elastic-scattering cross sections above 100 keV. Below this incident energy, however, the FC and MC results even for elastic scattering begin to deviate significantly, resulting in a 20% difference between the two at 10 keV. Unlike the elastic-scattering cross section, the FC and MC results for excitation and ionisation differ significantly across the entire incident energy range considered. More specifically, the MC results sit above the FC ones at all energies. At 30 keV, the MC CS-CCC results are 2.75 times larger than the FC ones for total excitation. Similarly, at 50 keV, the MC ionisation cross section is 1.4 times larger than the FC one. Such significant differences in the cross sections for excitation and ionisation resulting from the FC and MC approaches can be understood by comparing the dipole polarisabilities from the two models. In the FC model we obtain a value of $6.98 a_0^3$, while as previously mentioned in Sec. III, the MC model produces a value of $11.66 a_0^3$ which is accurate and 1.67 times larger than the FC one. Putting all of these observations together, it is clear that modelling $\bar{p} + \text{C}$ collisions using the FC target-structure model is not sufficient to accurately produce the elastic-scattering, excitation, and ionisation cross sections. There are two main reasons for this. The first is that the FC approach does not account for all of the valence-valence and core-valence electron correlations, which are crucial and must be taken into account when modelling the collisions at lower incident energies. The second reason is that the FC method does not include core-excitation and autoionising states in the close-coupling calculations. As we will see below, they make up a significant portion of the total excitation and ionisation cross sections.

As can be seen in the bottom panel of Fig. 2, the MC CS-CCC results for the ionisation cross section are lower than both sets of BGM calculations by Lüdde *et al.* [19] below 300 keV. The largest difference between the MC CS-CCC results and the BGM ones with the no-response model occurs at 10 keV, where the former is about 50% smaller than the latter. There is a smaller, albeit still significant, difference between the MC CS-CCC and BGM results with the response model, which is at most about 40%. As the incident energy increases above 300 keV, the difference between the three sets of results decreases. We note that the BGM calculations were done using an independent-particle model as well as the independent-event model to calculate the net ionisation [19].

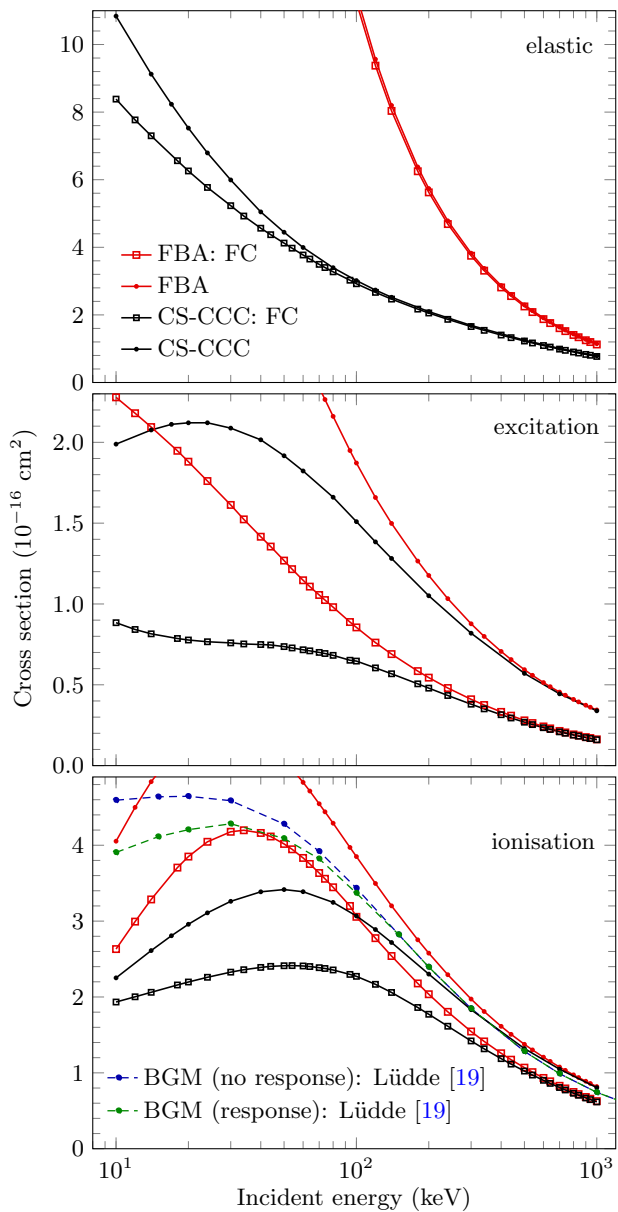


FIG. 2. Cross sections for elastic scattering (top panel), total excitation (middle panel), and ionisation (bottom panel) in $\bar{p} + \text{C}$ collisions. The present CS-CCC and FBA results obtained using both the FC and MC target structure models are shown. The BGM results by Lüdde *et al.* [19] for net ionisation are also shown for comparison.

The cross sections for target-excitation to states of C which can be described using both the FC and MC approaches are presented in Fig. 3 (obviously, the MC spectrum is much richer). As done in Fig. 2, for comparison FBA calculations with both target structure models are also presented. The top panel shows the cross sections for excitation of the $2s^2 2p 3s^3 P^o$ state, the middle panel for the $2s^2 2p 3p^3 P^e$ state, and the bottom panel for the $2s^2 2p 3p^3 D^e$ state. Similar to what we

have already seen in Fig. 2, both the FC and MC sets of results from the FBA calculations merge with the CS-CCC ones at high incident energies for all the transitions. Furthermore, as can be seen in the bottom panel, the CS-CCC and FBA cross sections (both FC and MC) for excitation of the $2s^2 2p 3p \ ^3D^e$ state all merge together at about 70 keV incident energy and above. Similarly, we see the same behaviour for excitation of the $2s^2 2p 3p \ ^3P^e$ state, although at a much higher incident energy, just below 1000 keV. At the same time, looking at the high energy limit for the cross section corresponding to the excitation of the $2s^2 2p 3s \ ^3P^o$ state, we see that the FC and MC approaches do not merge at all. As this transition is a dipole-allowed one, we can look at the oscillator strength for this transition to understand why this is the case. The FC model produces an oscillator strength for the $2s^2 2p^2 \ ^3P^e \rightarrow 2s^2 2p 3s \ ^3P^o$ transition of 0.102, meanwhile as seen in Table III, the MC model produces a value of 0.130, which is in a much better agreement the accepted value [41]. It is well known that in the high energy limit, the FBA cross section for dipole allowed transitions is proportional to the corresponding oscillator strength [47]. Therefore, we expect to see roughly a similar level of difference between the cross sections using the FC and MC approaches as those seen in their respective oscillator strengths. This is indeed found to be the case since the oscillator strength from the MC model is 1.27 times larger than the FC one, meanwhile the corresponding cross section is 1.47 times larger.

In Fig. 4 we present the cross sections of excitation to the $2s 2p^3 \ ^3D^o$, $2s 2p^3 \ ^3P^o$, and $2s 2p^3 \ ^3S^o$ states of the C target. These collectively represent a set of core-excitation states, where one of the inner-shell electron is excited to the valence shell. Alongside the CS-CCC results, we also give the present FBA calculations. Here, there are no FC results to compare to, as the FC model does not include core-excited states. For these transitions, the CS-CCC and FBA results also merge at high incident energies like observed in the previous figures, displaying a consistent behaviour in all the results we have presented.

An interesting observation can be made by comparing the magnitude of the cross sections for excitation to the $2s 2p^3 \ ^3D^o$ and $2s 2p^3 \ ^3P^o$ states to the total excitation cross section, shown in the middle panel of Fig. 2. For example, at 20 keV incident energy, the sum of these two core-excitation cross sections is $1.08 \times 10^{-16} \text{ cm}^2$, whereas the total excitation cross section is $2.07 \times 10^{-16} \text{ cm}^2$. This shows that at the peak of this cross section, the contribution from excitation of core electrons can be as high as 50%. This seems to indicate that at least at lower incident energies, one of the main reasons why the FC and MC results, shown in the middle panel of Fig. 2, differ is the fact that the FC model does not include these important states in the coupled-channel calculations. Lastly, it is worth pointing out that the $2s 2p^3 \ ^3S^o$ state is autoionising, meaning that it is situated above the first ionisation threshold of the C atom and

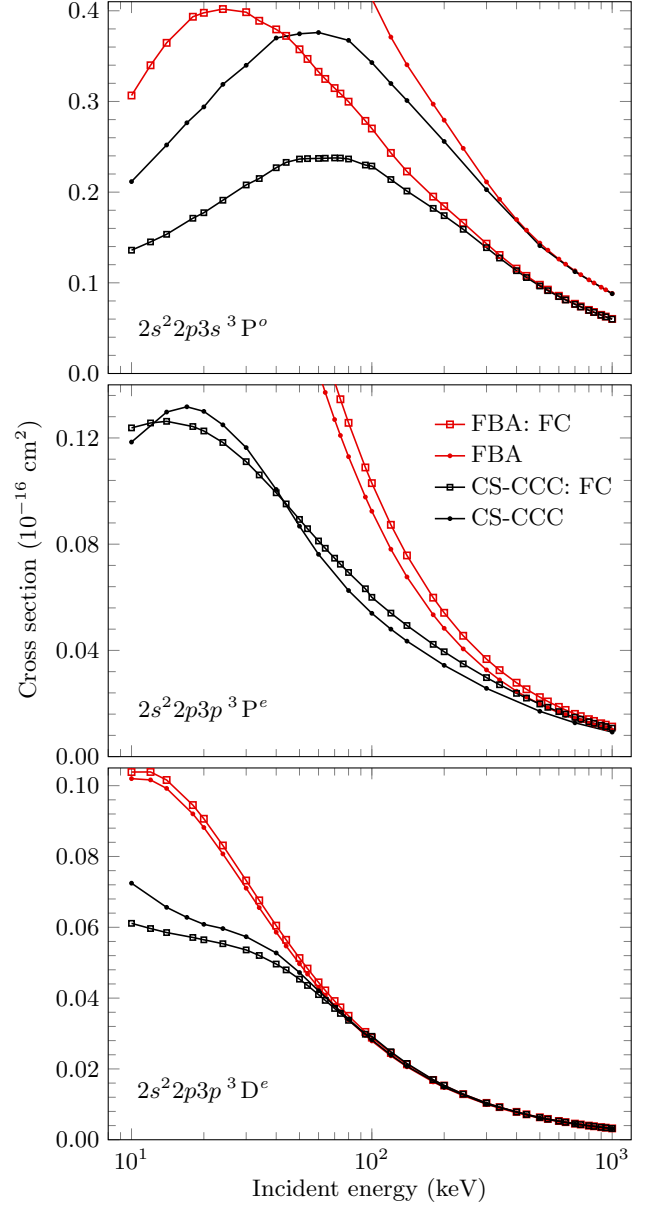


FIG. 3. Cross sections of excitation to the $2s^2 2p 3s \ ^3P^o$ (top panel), $2s^2 2p 3p \ ^3P^e$ (middle panel), and $2s^2 2p 3p \ ^3D^e$ (bottom panel) states of C. The present CS-CCC and FBA results obtained using both the FC and MC target structure models are shown.

contributes to the ionisation cross section presented in the bottom panel of Fig. 2. Thus, this excitation to this state alone is responsible for about 7% of the ionisation cross section at its peak, further emphasising the importance of having a MC description of the C atom when modelling $\bar{p} + \text{C}$ collisions.

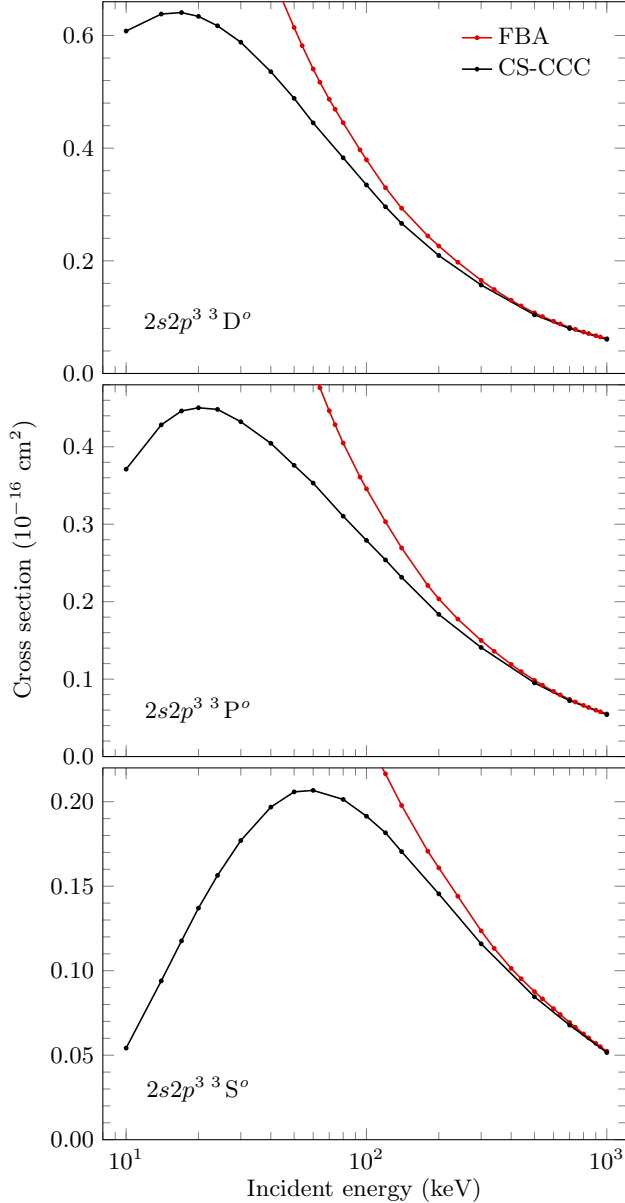


FIG. 4. Cross sections of excitation to the $2s2p^3\ ^3D^o$ (top panel), $2s2p^3\ ^3P^o$ (middle panel), and autoionising $2s2p^3\ ^3S^o$ (bottom panel) states of C. The present CS-CCC and FBA results obtained using both the FC and MC target structure models are shown.

V. CONCLUSIONS AND OUTLOOK

In this work we have developed a single-centre Coulomb-Sturmian-based convergent close-coupling method to study collisions with arbitrary multi-electron targets. We have done this using the LS coupling scheme and by introducing a new atomic structure code that seamlessly incorporates into our semi-classical CS-CCC code suite. This software is capable of generating structure models with an arbitrary number of frozen

and active electrons making it very robust and flexible. Using the set of pseudostates generated by this program, we can then expand the total scattering wavefunction that describes a heavy ion collision with the target atom of interest. Substituting this expansion into the full Hamiltonian of the collision system, we obtain a set of coupled-channel equations for the expansion coefficients which is solved to determine the cross sections for any collision process of interest.

To demonstrate the capabilities of this new extension to the CS-CCC method, we have applied it to study $\bar{p} + C$ collisions. The structure model we developed to represent the C atom agree very well with the NIST data available [41] for both the excitation energies and oscillator strengths of the first several excited states. Furthermore, the dipole polarisability of the ground state of the C atom produced by this model is within 3% of the accepted value. The practical advantage of our structure model is that, in addition to accurate bound states, it generates pseudostates which span the continuous spectrum indicating that the present structure model is accurate and suitable for subsequent close-coupling calculations to be performed. Within the incident energy range of 10 keV to 1000 keV, we have presented cross sections for elastic scattering, total excitation, and ionisation. We have also presented a set of state-resolved cross sections for excitation to states that can be described using both the FC and MC models and some core-excitation states which can only be described using the MC model.

Carbon is one of the most abundant elements in the universe. It is also one of the common atomic building blocks in biologically relevant molecules. This makes studying collisions involving C, and molecular targets that contain carbon atoms, crucial for the further development of hadron therapy for cancer treatment [48]. The present results can be used to benchmark and encourage further studies of $\bar{p} + C$ collisions. This newly developed theory is the first necessary step towards studying collisions involving other projectiles such as protons and other positively charged ions, where electron capture by the projectile is possible. Furthermore, this development of the CS-CCC method opens the door to studying a whole new set of ion collisions with other multi-electron targets, including impurity ions, of interest to plasma diagnostics [49], astrophysics [50] and hadron therapy applications [51] which was not possible with the previous implementations of the CCC approach to ion-atom scattering. Finally, it must be emphasised that even the current single-centre version of the CS-CCC method can be used to calculate electronic excitations and electron loss in proton and other highly charged ion collisions with multi-electron targets by simply increasing the basis size. When the size of the basis is large enough, the cross sections for excitation of the lowest states and total electron loss will be sufficiently accurate.

ACKNOWLEDGMENTS

This work was supported by the Australian Research Council. We acknowledge the resources provided by Pawsey Supercomputer centre, and the National

Computing Infrastructure. N.W.A. acknowledges support through Australian Government Research Training Program Scholarships. We thank Prof. Tom Kirchner for providing the theoretical data of Ref. [19] in tabulated form.

-
- [1] C. Hill, Dipti, K. Heinola, A. Dubois, N. Sisourat, A. Taoutioui, H. Agueny, K. Tőkési, I. Ziaean, C. Illescas, A. Jorge, L. Méndez, A. Kadyrov, N. Antonio, A. Kotian, T. Kirchner, A. Leung, J. Ko, J. Lee, O. Marchuk, M. O’Mullane, E. Litherland-Smith, G. Pokol, O. Asztalos, P. Balazs, Y. Wu, C. Jia, L. Liu, and J. Wang, *Nucl. Fusion* **63**, 125001 (2023).
 - [2] L. Gu and C. Shah, “Charge exchange in x-ray astrophysics,” (Springer Nature Singapore, 2023) pp. 255–289.
 - [3] D. Belkić, *J. Math. Chem.* **47**, 1366 (2010).
 - [4] A. C. Kraan, *Front. Oncol.* **5** (2015), 10.3389/fonc.2015.00150.
 - [5] S. Rossi, *Physics* **4**, 229 (2022).
 - [6] H. V. Knudsen, M. H. Holzscheiter, N. Bassler, J. Alsner, G. Beyer, J. J. DeMarco, M. Doser, D. Hajdukovic, O. Hartley, K. S. Iwamoto, O. Jäkel, S. Kovacevic, S. P. Møller, J. Overgaard, J. B. Petersen, O. Ratib, T. D. Solberg, S. Vranjes, and B. G. Wouters, *Nucl. Instrum. Method Phys. Res. Sect. B: Beam Interact. Mater. At.* **266**, 530 (2008).
 - [7] Z. Dimcovski and M. Doser, (2025), 2503.24158v1.
 - [8] A. Chattaraj and T. P. Selvam, *Phys. Med. Bio.* **67**, 185014 (2022).
 - [9] H. J. Lüdde, M. Horbatsch, and T. Kirchner, *Phys. Rev. A* **106**, 022813 (2022).
 - [10] R. E. Olson, A. Salop, R. A. Phaneuf, and F. W. Meyer, *Phys. Rev. A* **16**, 1867 (1977).
 - [11] I. M. Cheshire, *Proc. Phys. Soc.* **84**, 89 (1964).
 - [12] M. Kimura and N. F. Lane, “The low-energy, heavy-particle collisions—a close-coupling treatment,” (Elsevier, 1989) pp. 79–160.
 - [13] T. G. Winter, *Phys. Rev. A* **33**, 3842 (1986).
 - [14] D. R. Schultz, M. R. Strayer, and J. C. Wells, *Phys. Rev. Lett.* **82**, 3976 (1999).
 - [15] D. Belkić, I. Bray, and A. Kadyrov, *State-of-the-Art Reviews on Energetic Ion-Atom and Ion-Molecule Collisions* (WORLD SCIENTIFIC, 2019).
 - [16] M. Schultz, *Ion-Atom Collisions* (De Gruyter, 2019).
 - [17] L. Tribedi, *Advances in Atomic Molecular Collisions* (Springer Nature Singapore, 2024).
 - [18] I. B. Abdurakhmanov, N. W. Antonio, M. Cytowski, and A. S. Kadyrov, “Portable gpu implementation of the wp-ccc ion-atom collisions code,” (Springer Nature Switzerland, 2025) pp. 102–114.
 - [19] H. J. Lüdde, M. Horbatsch, and T. Kirchner, *Phys. Rev. A* **104**, 032813 (2021).
 - [20] T. Kirchner, M. Horbatsch, H. J. Lüdde, and R. M. Dreizler, *Phys. Rev. A* **62**, 042704 (2000).
 - [21] C. C. Jia, J. W. Gao, Y. Wu, J. G. Wang, and N. Sisourat, *Phys. Rev. A* **110**, 012803 (2024).
 - [22] I. B. Abdurakhmanov, A. S. Kadyrov, I. Bray, and A. T. Stelbovics, *J. Phys. B: At. Mol. Opt. Phys.* **44**, 075204 (2011).
 - [23] S. K. Avazbaev, A. S. Kadyrov, I. B. Abdurakhmanov, D. V. Fursa, and I. Bray, *Phys. Rev. A* **93**, 022710 (2016).
 - [24] I. B. Abdurakhmanov, A. S. Kadyrov, S. K. Avazbaev, and I. Bray, *J. Phys. B: At. Mol. Opt. Phys.* **49**, 115203 (2016).
 - [25] I. B. Abdurakhmanov, J. J. Bailey, A. S. Kadyrov, and I. Bray, *Phys. Rev. A* **97**, 032707 (2018).
 - [26] N. W. Antonio, I. Bray, and A. S. Kadyrov, *Phys. Rev. A* **110**, 032810 (2024).
 - [27] S. U. Alladustov, I. B. Abdurakhmanov, A. S. Kadyrov, I. Bray, and K. Bartschat, *Phys. Rev. A* **99**, 052706 (2019).
 - [28] K. H. Spicer, C. T. Plowman, N. W. Antonio, M. S. Schöffler, M. Schulz, and A. S. Kadyrov, *Phys. Rev. A* **109**, 062805 (2024).
 - [29] I. B. Abdurakhmanov, A. S. Kadyrov, D. V. Fursa, S. K. Avazbaev, J. J. Bailey, and I. Bray, *Phys. Rev. A* **91**, 022712 (2015).
 - [30] I. B. Abdurakhmanov, C. Plowman, A. S. Kadyrov, I. Bray, and A. M. Mukhamedzhanov, *J. Phys. B: At. Mol. Opt. Phys.* **53**, 145201 (2020).
 - [31] I. B. Abdurakhmanov, C. T. Plowman, K. H. Spicer, I. Bray, and A. S. Kadyrov, *Phys. Rev. A* **104**, 042820 (2021).
 - [32] I. B. Abdurakhmanov, A. S. Kadyrov, D. V. Fursa, and I. Bray, *Phys. Rev. Lett.* **111**, 173201 (2013).
 - [33] I. B. Abdurakhmanov, A. S. Kadyrov, D. V. Fursa, S. K. Avazbaev, and I. Bray, *Phys. Rev. A* **89**, 042706 (2014).
 - [34] C. T. Plowman, I. B. Abdurakhmanov, I. Bray, and A. S. Kadyrov, *Eur. Phys. J. D* **76** (2022), 10.1140/epjd/s10053-022-00359-w.
 - [35] C. F. Fischer, T. Brage, and P. Jönsson, *Computational Atomic Structure* (Routledge, 2019).
 - [36] M. Rotenberg, “Theory and application of sturmian functions,” (Elsevier, 1970) pp. 233–268.
 - [37] I. B. Abdurakhmanov, A. S. Kadyrov, and I. Bray, *Phys. Rev. A* **94**, 022703 (2016).
 - [38] N. W. Antonio and A. S. Kadyrov, *Phys. Rev. A* **111**, 052806 (2025).
 - [39] C. Froese Fischer, *Comput. Phys. Commun.* **43**, 355 (1987).
 - [40] J. Avery and J. Avery, *Generalized Sturmians and Atomic Spectra* (World Scientific Publishing Co. Pte. Ltd., 2006).
 - [41] A. Kramida, Yu. Ralchenko, J. Reader, and NIST ASD Team, NIST Atomic Spectra Database (ver. 5.12), [Online]. Available: <https://physics.nist.gov/asd> [2025, June 30]. National Institute of Standards and Technology, Gaithersburg, MD. (2024).
 - [42] S. Nasiri, S. Bubin, and L. Adamowicz, *Mol. Phys.* **122** (2024), 10.1080/00268976.2024.2325049.
 - [43] Y. Wang, O. Zatsarinny, and K. Bartschat, *Phys. Rev. A* **87**, 012704 (2013).

- [44] V. Stancalie, *J. Phys.: Conf. Ser.* **576**, 012010 (2015).
- [45] O. Zatsarinny, *Comput. Phys. Commun.* **174**, 273 (2006).
- [46] P. Schwerdtfeger and J. K. Nagle, *Mol. Phys.* **117**, 1200 (2019).
- [47] B. H. Bransden and M. R. C. McDowell, *Charge Exchange and the Theory of Ion-Atom Collisions* (Oxford University Press Oxford, 1992).
- [48] E. Erdmann, M.-C. Bacchus-Montabonel, and M. Labuda, *Phys. Chem. Chem. Phys.* **19**, 19722 (2017).
- [49] J. Snipes, L. Baylor, A. Bortolon, F. Effenberg, E. Gilson, A. Loarte, R. Lunsford, R. Maingi, S. Meitner, F. Nespoli, S. Maruyama, A. Nagy, Z. Sun, J. Ulreich, and T. Wauters, *Nucl. Mater. Energy* **41**, 101809 (2024).
- [50] W. R. Thompson, M. B. Shah, and H. B. Gilbody, *J. Phys. B: At. Mol. Opt. Phys.* **29**, 725 (1996).
- [51] H. Nikjoo, S. Uehara, D. Emfietzoglou, and A. Brahme, *New J. Phys.* **10**, 075006 (2008).